Effective emissivities of isothermal blackbody cavities calculated by the Monte Carlo method using the three-component bidirectional reflectance distribution function model

Alexander Prokhorov

Virial International, LLC, 538 Palmspring Drive, Gaithersburg, Maryland 20878, USA (avpro@virial.com)

Received 11 October 2011; revised 23 December 2011; accepted 23 December 2011; posted 3 January 2012 (Doc. ID 156376); published 1 May 2012

This paper proposes a three-component bidirectional reflectance distribution function (3C BRDF) model consisting of diffuse, quasi-specular, and glossy components for calculation of effective emissivities of blackbody cavities and then investigates the properties of the new reflection model. The particle swarm optimization method is applied for fitting a 3C BRDF model to measured BRDFs. The model is incorporated into the Monte Carlo ray-tracing algorithm for isothermal cavities. Finally, the paper compares the results obtained using the 3C model and the conventional specular-diffuse model of reflection.

OCIS codes: 120.5630, 230.6080, 290.1483.

1. Introduction

Near-isothermal-heated cavity is a source of optical radiation whose characteristics approach those of the perfect blackbody. Therefore, it can be computed using the fundamental laws of physics. Blackbody cavities are widely used as calibration sources in optical radiometry, photometry, and radiation thermometry [1,2]. The most important characteristic of a blackbody cavity is its effective emissivity. In other words, unlike a flat surface, radiation emerging from every point of cavity's internal surface comprises radiation emitted by all other points that is reflected by the point under consideration. High-quality blackbodies have small temperature nonuniformity and usually can be considered isothermal. An isothermal cavity in a nonemitting environment holds thermodynamic equilibrium. According to generalized Kirchhoff's law [3], the effective emissivity of a cavity with opaque isothermal walls can be expressed in terms of its effective reflectance ρ_e and does not depend on the cavity temperature. Spectral local directional effective emissivity of isothermal cavity can be determined as

$$\varepsilon_e(\lambda, \boldsymbol{\xi}, \boldsymbol{\omega}) = 1 - \rho_e(\lambda, \boldsymbol{\xi}, \boldsymbol{\omega}), \tag{1}$$

where λ is the wavelength, and $\boldsymbol{\xi}$ and $\boldsymbol{\omega}$ are positional and directional vectors, respectively.

The effective emissivity of isothermal cavity depends on its geometrical parameters and the registration conditions of the cavity's radiation, as well as the optical properties of cavity walls. The integration of the spectral local directional effective emissivity over the spectral, spatial, or angular domain gives specific effective emissivity values (e.g., integration over a conical solid angle leads to a conical effective emissivity and so forth).

The effective emissivity of blackbody radiation sources must be known with the uncertainty small enough to conduct reliable calibration of various types of detectors, radiometers, radiation thermometers, and other measuring devices. Measuring the effective emissivity is difficult, requires special measurement equipment, and frequently can be

1559-128X/12/132322-11$15.00/0

performed only in thermal and geometrical conditions, which do not adequately reproduce real operating conditions of blackbody radiators. Therefore, calculations of radiation characteristics for blackbody cavities are necessary at the design stage as well as at the stage of metrological characterization.

Various methods for calculating the effective emissivity have been developed since the second half of the 20th century (their synopses can be found in [4,5]). Most of them have a limited area of applicability or use overly simplified models to account for optical properties of cavity walls. The Monte Carlo ray-tracing method is the most flexible and has been applied to effective emissivity calculations for cavities of various shapes [5–7]. This method uses ray optics, so phenomena such as polarization and diffraction are out of the scope of this work.

2. Optical Properties of Radiating Cavity Materials

The choice of material or coating of radiating blackbody cavities is determined by many parameters: operational temperature of a blackbody, required effective emissivity, cavity shape, and geometrical conditions of collecting the radiation emitted by a cavity. Blackbodies operating at low temperatures have radiating cavities internally coated with various black paints like those used for thermal detector of optical radiation [8–11]. High-temperature blackbodies usually are made of graphite or other refractory materials [12]. Blackbodies of intermediate temperatures frequently have an oxidized metallic surface. Spectral range, in which the material should be employed, depends on the blackbody operating temperature.

Unfortunately, the optical properties of materials and coatings used for radiating surfaces of blackbodies have been insufficiently studied. Their optical constants (complex refractive indices) very often are unknown. Moreover, the optical properties of such materials are determined by not only the optical constants but also the condition of the surface (roughness, granularity and treatment), Because of the presence of many uncontrolled parameters in the published data for the sample under consideration, characterization of each particular sample is necessary.

Effective emissivities depend to a great extent upon the angular distribution of the radiation reflected by the internal surface of the cavity. This distribution is the measurable optical characteristic of the material and can be described by the bidirectional reflectance distribution function (BRDF) introduced by Nicodemus *et al.* [13]. In the spherical coordinate system in Fig. 1, BRDF, $f_r[\mathrm{sr}^{-1}]$, is defined as

$$f_r(\lambda,\theta_i,\phi_i,\theta_v,\phi_v)=\frac{dL_{\lambda,v}(\lambda,\theta_i,\phi_i,\theta_v,\phi_v)}{dE_{\lambda,i}(\lambda,\theta_i,\phi_i)}, \qquad (2)$$

where θ and ϕ are the polar and azimuthal angles, respectively, L_λ is the spectral radiance, and E_λ is the spectral irradiance. Subscripts i and v refer to incidence and viewing directions, respectively.

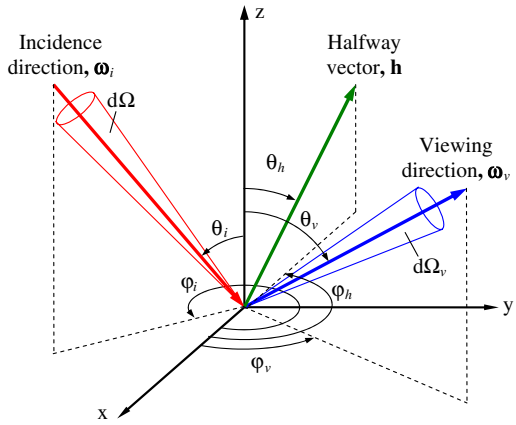

Fig. 1. (Color online) Schematic for the BRDF definition.

It is supposed that fluorescence and translucency are absent. Without the loss of generality, here and hereinafter, we will consider the case of monochromatic radiation and omit dependence on the wavelength as well as the adjective "spectral." The direct use of BRDF measurements for calculations of effective emissivities is problematic due to incompleteness of experimental data: most BRDF measurements are performed only in the plane of incidence (so-called in-plane BRDF) and for several incidence angles only. Thus, it usually is necessary to introduce BRDF models in the form of analytical functions. A number of such models were developed for computer graphics, digital image synthesis, and remote sensing during the past two decades [14–22].) Among these models, there are physically based (i.e., describing real physical phenomena such as a reflection of optical radiation from randomly rough surfaces or volumetric scattering in translucent media) as well as empirical or semi-empirical models, which is only mathematical formulas with a set of tunable parameters. Many of these models cannot be used in precise radiometric calculations due to their limitations. Some are only oriented to plausible visual perception while others poorly reproduce reflective behavior of real materials or reproduce it satisfactorily for not all combinations of incidence and viewing angles.

In the radiative heat transfer analysis, the most widespread (and straightforward) reflection model is the specular-diffuse model [23]. It calculates the angular distribution of reflected radiation as the sum of a perfect diffuse (Lambertian) and a perfect specular component. It is assumed that both components do not depend on incidence angle. Like Ono [6], we will call this model uniform specular-diffuse (USD) to distinguish it from its modification where a specular component depends on an incidence angle [7]. A USD model contains only two parameters: the directional–hemispherical reflectance (DHR) ρ, and the diffusity $D=\rho_d/\rho$, where ρ_d is the diffuse reflectance. The USD reflection model is the most popular in the Monte Carlo ray-tracing algorithms due to the simplicity of its implementation and minimal number of tuning parameters. However, the USD model has two drawbacks: there is no objective

criterion for subdivision of reflectance onto diffuse and specular components, and fitting to the measured BRDF is impossible because the BRDF of a perfectly specular component is the Dirac δ-function that has infinite value if $\theta_v = \theta_i$ and $\phi_v = \phi_i \pm \pi$. Real-world specularly reflecting materials of blackbody cavities have specular peaks of small, but finite, widths and large, but finite, BRDF maxima. We will call such materials quasi-specular.

Analysis of BRDF measurements at ambient temperatures [8–11,24,25] for some black coatings and graphite samples [26] shows the USD model might be too crude an approximation for these data but can be represented as the sum of three components: near-Lambertian (diffuse), almost specular (quasi-specular), and glossy (having wide forward-scattering lobe). To our knowledge, BRDF measurements for graphite at temperatures about or above 1000 K, that is at operational temperatures of graphite blackbodies, have never been performed.

Here, the names of components are not concerned with physical phenomena they determine but refer to their shapes only. For example, diffuse component might be caused by multiple scattering on the surface roughnesses, or by volumetric scattering inside a translucent coating and so forth. The challenge is to develop a simple BRDF model that satisfies the following requirements.

(1) The BRDF model must obey the reciprocity principle:

$$f_r(\theta_i, \phi_i, \theta_v, \phi_v) = f_r(\theta_v, \phi_v, \theta_i, \phi_i). \tag{3}$$

(2) The BRDF model must obey the energy conservation law, i.e., DHR

$$\rho(\theta_i) = \int_{\phi_v=0}^{2\pi} \int_{\theta_v=0}^{\pi/2} f_r(\theta_i,\phi_i,\theta_v,\phi_v) \sin\theta_v \cos\theta_v \mathrm{d}\theta_v \mathrm{d}\phi_v \tag{4}$$

must be less than 1 for any incidence angle θ_i; DHR dependence on θ_i computed using Eq. (4) must reproduce DHR behavior of a real material.

(3) The BRDF model must have enough tuning parameters to be fitted to the measured in-plane BRDF for all incidence angles for which it was measured.

(4) The BRDF model must be physically based to correctly predict BRDF values outside the range of measured incidence and viewing angles.

(5) It is desirable that the BRDF model will be suitable for importance sampling [27] (i.e., for generating randomly reflected rays with the probability density function coordinated with the BRDF values). Importance sampling substantially accelerates convergence of Monte Carlo computations.

The objectives of this work are fivefold:

1. to construct the BRDF model which satisfies the above-mentioned requirements,
2. to investigate the model's features,
3. to develop the algorithm for fitting modeled BRDF to measured values,
4. to incorporate this model into the ray-tracing algorithm for effective emissivity calculation, and
5. to compare the results obtained using this model with those for the USD model of reflection.

The principal aim is to develop a model that mimics BRDF behavior of materials of blackbody cavities better than the specular-diffuse model does.

Since the different physical mechanisms may be responsible for reflection from various materials of blackbody cavities or even be superimposed, it is hardly possible to employ one certain existing BRDF model to describe the reflection characteristics of all materials considered. We used a phenomenological approach rather than the first principle-based theoretical approach. Analysis of available experimental data [8–11,24–26] shows that one can represent BRDF, f_r, by the linear combination of diffuse, $f_{r,d}$, quasi-specular, $f_{r,qs}$, and glossy, $f_{r,g}$, components:

$$f_r = k_d f_{r,d} + k_{qs} f_{r,qs} + k_g f_{r,g}, \tag{5}$$

where k_d, k_{qs}, and k_g are nonnegative and

$$k_d + k_{qs} + k_g = 1. \tag{6}$$

Diffuse component corresponds to reflected radiation more or less uniformly scattered within the hemispherical solid angle. Lambertian reflection (also known as ideal diffuse or perfectly diffuse reflection) is the extreme case of diffuse reflection when $f_{r,d} = \text{const}$. A quasi-specular component has a very narrow but finite width peak in the direction of perfectly specular (mirrorlike) reflection. A glossy component is similar to the quasi-specular component but is wider so that it forms a specular lobe rather than a peak. It is obvious that f_r will obey the reciprocity principle and energy conservation law if this takes place for $f_{r,d}$, $f_{r,qs}$, and $f_{r,g}$. Analysis of numerous particular BRDF models shows that the majority of them do not comply with five requirements expounded above. We considered only isotropic BRDF models depending on $\phi = |\phi_i - \phi_v|$ instead of ϕ_i and ϕ_v. For anisotropic BRDF models, only their isotropic versions were considered.

It was found that the model proposed by Geisler-Moroder and Dür [28] can be employed for both quasi-specular and glossy components. The Rahman–Pinty–Verstraete (RPV) reflection model and its modifications [18] show good fitting results for various diffuse samples. However, these models are nonnormalized (i.e., require additional efforts to preserve energy conservation). Since Lambertian reflectance can be considered as a special case of this family of models, we decided that the Lambertian BRDF will be a reasonable trade-off for a diffuse component in our model.

3. Three-Component Bidirectional Reflectance Distribution Function Model

Using this approach, we introduced the three-component bidirectional reflectance distribution function (3C BRDF) model as an improvement of the USD model. The BRDF of the diffuse (Lambertian) component is the constant:

$$f_{r,d} = \frac{R_d}{\pi}, \tag{7}$$

where R_d is the diffuse reflectance (DHR) of the diffuse component.

For quasi-specular and glossy components, the model proposed by Geisler-Moroder and Dür [28] for rough surfaces has been chosen in its isotropic version:

$$f_r(\theta_i, \theta_v, \phi) = \frac{R(\theta_h)}{\pi\sigma} \exp\left[-\left(\frac{\tan\theta_h}{\sigma}\right)^2\right] \times \frac{2[1 + \cos\theta_i \cos\theta_v - \sin\theta_i \sin\theta_v \cos\phi]}{(\cos\theta_i \cos\theta_v)^4}, \tag{8}$$

where σ is the roughness parameter and θ_h is the halfway angle (Fig. 1).

This BRDF model is based on the microfacet model of reflection [29]. The last multiplier allows us to avoid infinite BRDF values at $\theta_i = \theta_v = \pi/2$ and, at the same time, plays the role of normalization factor. Specular reflectance, R, of microfacet depends on the angle θ_h of the incidence onto the microfacet. This angle, called the halfway angle, is formed by the surface normal and the halfway vector $\mathbf{h} = \frac{\boldsymbol{\omega}_v - \boldsymbol{\omega}_i}{2\|\boldsymbol{\omega}_v - \boldsymbol{\omega}_i\|}$ (Fig. 1). It is assumed that microfacet normals have Gaussian distribution with zero mean value and standard deviation σ. The greater the σ the greater the surface roughness and, correspondingly, the wider the BRDF lobe. Elementary physical reasoning suggests that DHR of a microfacet model must equal 1 for all incidence angles if $R(\theta_h) \equiv 1$. DHRs, of all microfacet models that neglect multiple reflections among microfacets, deviate from 1 for such a case; the greater roughness, the greater this deviation.

The last term in Eq. (8) is constructed in such a way that the deviation of DHR from 1 at $R(\theta_h) \equiv 1$ is minimized (Fig. 2). Deviations become significant only for large σ and large θ_i. Since the reflectance of materials of blackbody cavities is essentially low, deviations of DHR computed by integration of BRDF in Eq. (8) from the actual DHR values will be substantially less.

The original model [28]) uses Schlick's approximation [30] of Fresnel's reflection law for unpolarized light:

$$R(\theta_h) = R_{qs} + (1 - R_{qs})(1 - \cos\theta_h)^5, \tag{9}$$

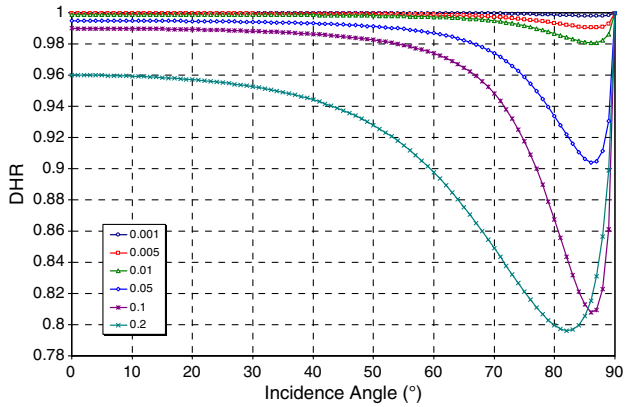

Fig. 2. (Color online) Dependences of the DHR on the incidence angle computed for the Geisler-Moroder and Dür BRDF model for $R = 1$ and $\sigma = 0.0001$, 0.005, 0.01, 0.05, 0.1, and 0.2 (see legend).

where R_{qs} is the specular reflectance of a microfacet at the normal incidence.

We also preferred Schlick's approximation over Fresnel's equation for the following reasons.

1. In the fitting problem, it is important to know a good initial value of a fitted parameter or at least the narrowest range of its acceptability. These data are unavailable *a priori* for the refractive index n and the extinction coefficient k while for the reflectance at the normal incidence, $0 \le R_{qs} \le 1$.
2. Fresnel's equation has more complicated form and comprises n^2 and k^2. These factors result in an increase of number of objective function minima and require introducing additional criteria to select the global minimum.
3. Although Eq. (8) is based on the microfacet model for rough surfaces, we found that one can apply this equation for modeling of reflection with a different scattering nature (e.g., subsurface or volumetric scattering for quasi-specular black paints). In such cases, parameters n and k can take uncommon values, lose their physical meaning, and should be considered as the fitting parameters only. Parameter R_{qs} remains within interval [0, 1] and maintains its physical meaning. Indeed, in such a case, σ in Eq. (8) should be considered only as a parameter determining the width of the BRDF lobe.
4. The Schlick formula not only approximates Fresnel's law accurately enough for dielectrics but also works several times faster.

For nondielectrics, Eq. (9) gives deviations from Fresnelian reflectance at large θ_h. However, large θ_h values usually correspond to very rough surfaces for which the effect of multiple reflections among microfacets overrides Schlick's approximation errors. The numerical experiments we performed did not reveal significant differences between the employment of Fresnel's law and Schlick's approximation for the tasks considered in this paper. The only drawback with Schlick's approximation, which hampers the

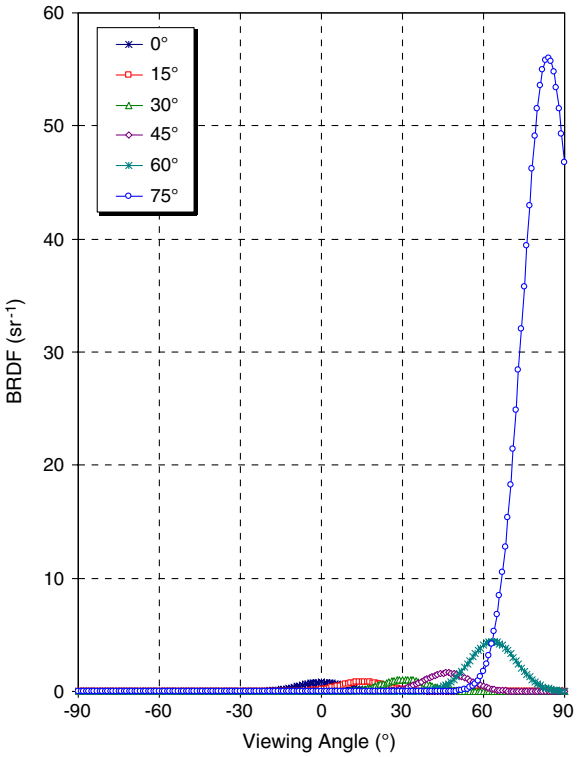

Fig. 3. (Color online) In-plane Cartesian plots for the Geisler-Moroder and Dür BRDF model with $R = 0.1$, $\sigma = 0.1$, and six incidence angles shown in legend. The negative values of viewing angles correspond to backscattering.

use of thr Geisler-Moroder and Dür model in the fitting problem, is nonzero reflectance that Eq. (9) gives for $R_{qs} = 0$ and $\theta_i > 0$. We were forced to add the condition $R(\theta_i) \equiv 0$ if $R_{qs} = 0$. From the formal point of view, this condition leads to mathematical discontinuity of $R(\theta_i)$, but computational experiments did not detect any erroneous or artifactual fitting results.

We used Eq. (8) for both quasi-specular and glossy components and allowed that $0.0001 \le \sigma_{qs} \le 0.01$ for the quasi-specular component and $0.01 < \sigma_g \le 0.5$ for the glossy BRDF component. In-plane BRDFs plotted in the Cartesian coordinate system according to Eqs. (8) and (9) for $R_g = 0.1$, $\sigma_g = 0.1$, and six values of θ_i (0°, 15°, 30°, 45°, 60°, and 75°) are shown in Fig. 3. The negative values of viewing angles θ_v correspond to the backscattering. The three-dimensional plots of glossy BRDFs expressed in relative units for $R_g = 0.1$ and $\sigma_g = 0.05$, 0.1 and 0.2 are presented in the spherical coordinate system in Fig. 4 for 45° of incidence.

DHR of the 3C BRDF model can be represented in the form

$$\rho(\theta_i) = \rho_d + \rho_{qs}(\theta_i) + \rho_g(\theta_i), \tag{10}$$

where every summand is the DHR of the appropriate component:

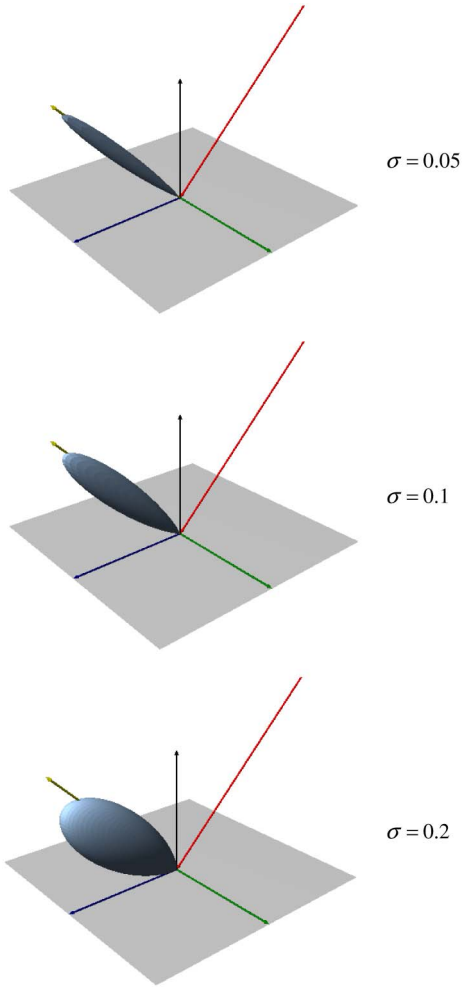

Fig. 4. (Color online) 3D plots in spherical coordinates for the Geisler-Moroder and Dür BRDF at the incidence angle of 45°; $R = 0.1$, $\sigma = 0.05$, 0.1, and 0.2.

$$\rho_d = k_d \int_{\phi_v=0}^{2\pi} \int_{\theta_v=0}^{\pi/2} f_{r,d}(R_d, \theta_i, \phi_i, \theta_v, \phi_v) \times \sin\theta_v \cos\theta_v \mathrm{d}\theta_v \mathrm{d}\phi_v = k_d R_d, \tag{11}$$

$$\rho_{qs}(\theta_i) = k_{qs} \int_{\phi_v=0}^{2\pi} \int_{\theta_v=0}^{\pi/2} f_{r,qs}(R_{qs}, \sigma_{qs}, \theta_i, \phi_i, \theta_v, \phi_v) \times \sin\theta_v \cos\theta_v \mathrm{d}\theta_v \mathrm{d}\phi_v, \tag{12}$$

and

$$\rho_g(\theta_i) = k_g \int_{\phi_v=0}^{2\pi} \int_{\theta_v=0}^{\pi/2} f_{r,g}(R_g, \sigma_g, \theta_i, \phi_i, \theta_v, \phi_v) \times \sin\theta_v \cos\theta_v \mathrm{d}\theta_v \mathrm{d}\phi_v. \tag{13}$$

The double integrals in Eqs. (12) and (13) were computed numerically using an adaptive

quadratures algorithm [31]. Our results agree with those obtained by the Monte Carlo integration [28]. For very small σ_{qs}, dependences $\rho_{qs}(\theta_i)$ practically coincide with appropriate Schlick's curves.

4. Fitting the 3C BRDF Model to BRDF Measurement Data

A. Goodness-of-Fit Criteria

The 3C model of reflection has eight parameters: k_d, R_d, k_s, R_s, σ_s, k_g, R_g, and σ_g. Three of them are interrelated as shown in Eq. (6). Besides, the following conditions must be fulfilled:

$$0 \le k_d, R_d, K_{qs}, R_{qs}, k_g, R_g \le 1, \tag{14}$$

$$0.0001 \le \sigma_{qs} \le 0.001, \tag{15}$$

$$0.001 < \sigma_g \le 0.5. \tag{16}$$

Mathematically, we deal with the problem of constrained optimization and have to find eight values of the 3C model parameters, which minimize distances between computed and measured BRDFs according to some goodness-of-fit criterion. Multiple numerical experiments did not help to isolate a unified criterion for all variety of BRDF shapes. For smooth BRDFs with the moderate dynamic range, the L_2 metric ensures good fitting results. The objective function F (K_d, R_d, k_{qs}, R_{qs}, σ_{qs}, k_g, R_g, σ_g) for the metric L_2 equals

$$F = \sum_{k=1}^{n_i} \sum_{j=1}^{n_{v,k}} [f_{r,m}(\theta_{i,k}, \theta_{v,jk}) - f_r(\theta_{i,k}, \theta_{v,jk})]^2, \tag{17}$$

where f_r and $f_{r,m}$ are computed and measured in-plane BRDF, n_i is the number of incidence angles, $n_{v,k}$ is the number of viewing angles in the BRDF measured at kth incidence angle $\theta_{i,k}$, and $\theta_{v,jk}$ is the jth viewing angle for the BRDF measured for $\theta_{i,k}$.

It was found that for very nonuniform BRDFs with a large dynamic range (for instance, for BRDF with a narrow quasi-specular peak), the C metric for relative deviations is more suitable:

$$F = \begin{cases} 0, \text{ if } f_{r,m}(\theta_{i,k}, \theta_{v,jk}) = f_r(\theta_{i,k}, \theta_{v,jk}) = 0 \\ \max\limits_{k=1,\ldots,n_i} \max\limits_{j=1,\ldots,n_{v,k}} \left\{ \frac{|f_{r,m}(\theta_{i,k}, \theta_{v,jk}) - f_r(\theta_{i,k}, \theta_{v,jk})|}{f_{r,m}(\theta_{i,k}, \theta_{v,jk}) + fr(\theta_{i,k}, \theta_{v,jk})} \right\} \text{ otherwise} \end{cases}. \tag{18}$$

For some intermediate cases, the best fit was achieved using the L_1 metric:

$$F = \sum_{k=1}^{n_i} \sum_{j=1}^{n_{v,k}} |f_{r,m}(\theta_{i,k}, \theta_{v,jk}) - f_r(\theta_{i,k}, \theta_{v,jk})|. \tag{19}$$

B. Optimization Algorithm

Numerical investigation has shown that the objective functions defined by Eqs. (17)–(19) have multiple minima but only one of them is the deepest. Therefore, we have to deal with multimodal objective functions and, correspondingly, with the global optimization problem. For such problems, the solution usually depends on a starting point. It was assumed that there is no a priori information, which would allow us to select a "good" starting point needed to detect the global minimum among several local minima. The particle swarm optimization (PSO) method [32] was chosen to solve this problem for two main reasons. First, PSO only requires knowledge of lower and upper allowed values for each variable instead of its "good" zero approximations. Second, PSO is applicable (at least, in principle) to the global optimization problem.

PSO is a stochastic, derivative-free, iterative optimization method that imitates random movement of "particles" in the multidimensional search space. The movements of the particles are determined by their individual best-known positions as well as the best-known position for a swarm as a whole. Although PSO does not guarantee locating the global minimum, the probability of its detection is high at the optimal tuning of the algorithm. We implemented the algorithm described in [33] conjugated with the normalization of parameters k_d, k_s and k_g for calculations of f_r after each iteration. A multiple restarts strategy was used to avoid stagnation and convergence to wrong solutions (local minima).

C. Practical Example

To demonstrate the practical application of the approach described above, we used BRDF measurements at the wavelength of 10.6 μm for the Chemglaze Z302 black coating reported in [24,25]. Fitting results, obtained using the objective function in Eq. (18), are presented in Fig. 5. The following values of 3C model were found: $k_d = 0.400$, $R_d = 0.003$, $k_{qs} = 0.408$, $R_{qs} = 0.091$, $\sigma_{qs} = 0.010$, $k_g = 0.191$, $R_g = 0.047$, and $\sigma_g = 0.072$. Figure 6 shows the computed DHR $\rho(\theta_i)$ together with ρ_d, $\rho_{qs}(\theta_i)$, and $\rho_g(\theta_i)$ for this model.

5. Monte Carlo Modeling Algorithm

The backward ray tracing [34] based on the reciprocity principle was implemented in the Monte Carlo algorithm for the effective emissivities calculations. Every ray starts outside the cavity; its starting position and direction are determined by the viewing conditions. For example, to compute the average normal effective emissivity that corresponds to the case of collecting cavity radiation using a very long focal-length optical system, rays have to be directed parallel to the cavity axis from points arbitrary distant from the cavity aperture and uniformly distributed across the circular section of the radiation beam.

For the case of a convergent or divergent ray beam emerging from the cavity aperture, conical effective

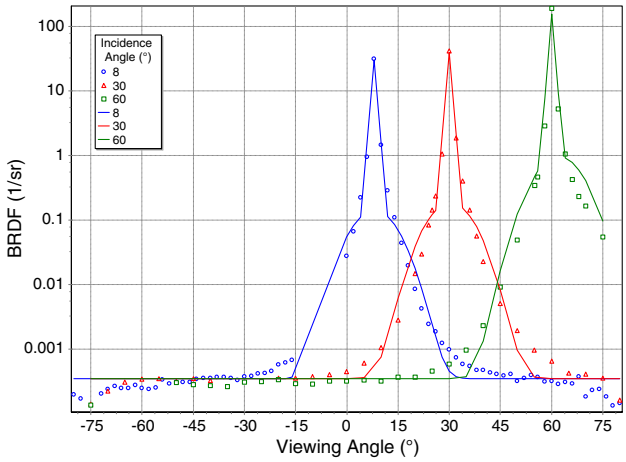

Fig. 5. (Color online) Results for the 3C BRDF model (lines) fitted to the Chemglaze Z302 black paint BRDFs measured at 10.6 μm (symbols).

emissivity that imitates viewing conditions with the objective lens or other imaging optical system, can be modeled by generating rays uniformly distributed within the conical solid angle and starting from the focal point (cone apex). If the starting point and the directional vector are known, one must solve the equation for a cavity surface together with parametric equations for a straight line. If the cavity consists of many surfaces, the line-surface intersection points have to be found for each surface. The true solution corresponds to the point that lies on some surface within its bounds and has the minimal distance from the starting point. We implemented this algorithm for cavities formed by the revolving of the non-self-intersecting polygonal line around the cavity axis.

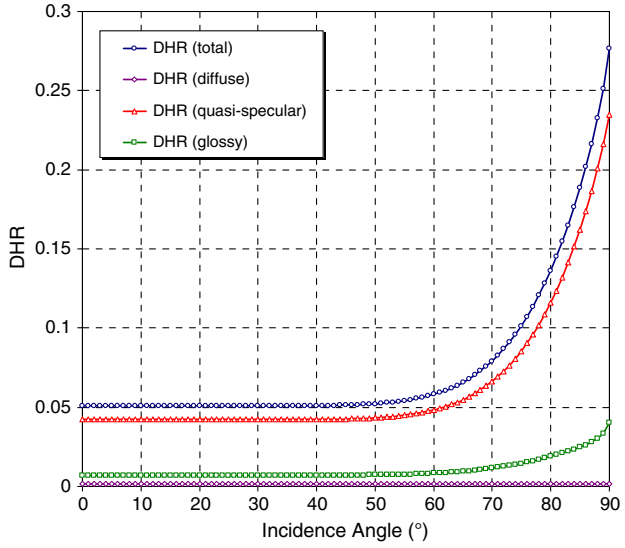

Fig. 6. (Color online) Dependences of the DHR on the incidence angle for 3C BRDF model (and its components, see the legend) fitted to the measured at 10.6 μm BRDFs for the Chemglaze Z302 black paint.

When a ray hits the cavity wall at an angle of incidence θ_i, the type of reflection is chosen using a random number u_r distributed uniformly from 0 to 1. If $u_r \le \rho_d(\theta_i)$, the diffuse reflection is chosen. If $u_r \le \rho_d(\theta_i) + \rho_{qs}(\theta_i)$, the reflection is quasi-specular; otherwise, the reflection is glossy. The statistical weight w defined by optical properties of a surface and a sampling algorithm for directions of reflection should be assigned to each reflected ray.

Importance sampling for diffuse component can be done using a well-known method [35]:

$$\sin^2 \theta_v = u_\theta, \tag{20}$$

$$\phi_v = 2\pi u_\phi, \tag{21}$$

where u_θ and u_ϕ are two random numbers from a uniformly distributed set between 0 and 1, θ_v and ϕ_v are the polar and azimuthal angles of a reflected ray in the local spherical coordinate system with the origin at the point of reflection and z axis coincident with the surface normal.

We used an alternative method that produces Cartesian coordinates of the unit vector directed along the reflected ray. The pair of uniformly distributed random numbers u_x and u_y are generated and accepted if $u_x^2 + u_y^2 < 1$, otherwise the new pair of u_x and u_y are generated. Cartesian coordinates of the unit reflection vector $\boldsymbol{\omega}_v$ in the local coordinate system are computed as

$$\begin{cases} \omega_x = 2u_x - 1 \\ \omega_y = 2u_y - 1 \\ \omega_z = +\sqrt{1 - \omega_x^2 - \omega_y^2} \end{cases}. \tag{22}$$

The statistical weight $w = R_d$ is assigned to the diffusely reflected ray.

The sampling procedure described in [28] was applied to quasi-specular and glossy components. First, spherical coordinates of the halfway vector $\mathbf{h}$ (Fig. 1) are computed using random numbers u_θ and u_ϕ:

$$\theta_h = \tan^{-1}(-\sigma \ln u_\theta) \tag{23}$$

and

$$\phi_h = 2\pi u_\phi. \tag{24}$$

Second, spherical coordinates have to be transformed to Cartesian coordinates:

$$\begin{cases} h_x = \sin\theta_h \cos\phi_h \\ h_y = \sin\theta_h \sin\phi_h \\ h_z = \cos\theta_h \end{cases}. \tag{25}$$

When coordinates of the halfway vector $\mathbf{h}$ are found, one can compute coordinates of the viewing

vector $\boldsymbol{\omega}_v$ specularly reflected from the microfacet with the normal $\mathbf{h}$ for the given incidence vector $\boldsymbol{\omega}_i$:

$$\begin{cases} \omega_{vx} = \omega_{ix} - 2(\boldsymbol{\omega}_i \cdot \mathbf{h})h_x \\ \omega_{vy} = \omega_{iy} - 2(\boldsymbol{\omega}_i \cdot \mathbf{h})h_y \\ \omega_{vz} = \omega_{iz} - 2(\boldsymbol{\omega}_i \cdot \mathbf{h})h_z \end{cases}. \tag{26}$$

According to the sampling procedure proposed in [31], the statistical weight

$$w = \frac{2R(\theta_h)}{1 - \omega_{iz}/\omega_{vz}} \tag{27}$$

is assigned to the reflected ray.

Each ray is traced until it escapes the cavity through the aperture. Ray weights decrease after each reflection; therefore, one can stop tracing of a ray if its weight becomes less than the required relative uncertainty γ of the effective emissivity calculation. To estimate the effective emissivity, a large number of rays should be traced; the estimator for effective emissivity is as follows:

$$\varepsilon_e = 1 - \frac{1}{n}\sum_{k=1}^{n}\prod_{j=1}^{m_k} w_{jk}, \tag{28}$$

where w_{jk} is the statistical weight of kth ray after jth reflection and m_k is the number of reflections in the trajectory of kth ray.

The algorithm described above can be modified for modeling nonisothermal cavities; however, this lies outside the scope of the present work.

6. Results of Numerical Experiments

A. Objectives of Numerical Experiments

The numerical experiments were aimed at investigating the specific effects of the angular dependence and finite width of BRDF profiles for quasi-specular and glossy components and identifying the situations when the 3C model of reflection lead to results that cannot be reproduced with the USD model for any values of ρ and D. For all numerical examples, cylindrical and cylindro-conical cavities were chosen (Fig. 7). Their geometrical parameters are: $r_c = 1$, $r_a = 0.5$, $l = 10$, $\beta = 30°$.

In all calculations presented below, 10^6 rays were traced with $\gamma = 10^{-6}$.

B. Cavity with Quasi-specular Walls

To investigate the difference between quasi-specular and perfectly specular reflection (an infinitely thin reflected ray in which energy does not depend on incidence angle), we compute the average normal effective emissivity as a function the viewing beam radius r for the cylindro-conical cavity shown in Fig. 7a. Elementary geometric consideration shows that, in the case of perfectly specular walls, a ray entering the aperture parallel to the cavity axis undergoes three successive reflections toward the apex of 30°-cone,

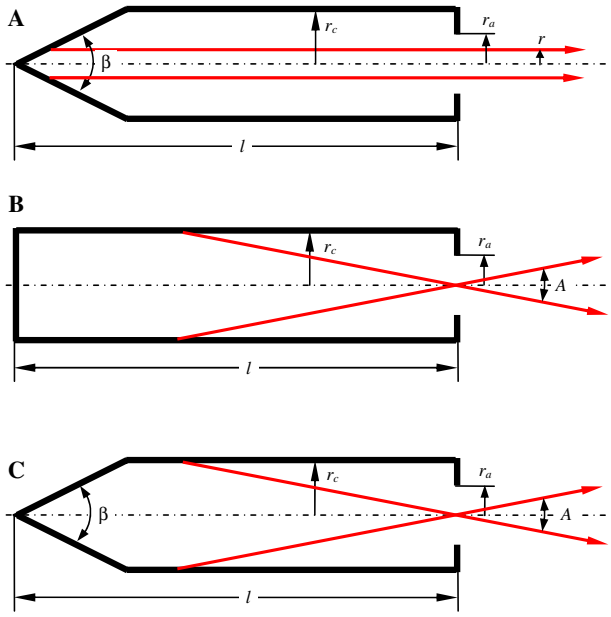

Fig. 7. (Color online) Schematics of the cavities and viewing conditions used for numerical experiments.

then reverses, and, after three reflections toward the aperture, escapes the cavity in the direction parallel to the cavity axis. Thus, if the specular reflectance of perfectly specular cavity walls equals 0.2, the local normal effective emissivity should be equal to $1 - (0.2)^6 = 0.999936$.

By assuming that the cavity walls are quasi-specular, we performed Monte Carlo modeling for $R_{qs} = 0.2$ and $\sigma_{qs} = 0.002$, 0.005, 0.007 and 0.01. Computed dependences are presented in Fig. 8. All effective emissivity values are less than 0.999936. This is explained by the following fact: effective emissivity is determined primarily by the radiance of the own thermal radiation of the directly viewable cavity wall area. In terms of the backward ray tracing, it means that the contribution of the first reflection is dominant. For the conical bottom having apex angle of 30°, a ray sent into the cavity parallel to its axis forms the incidence angle of 75° with the cavity bottom normal. According to Eq. (9), if $R_{qs} = 0.2$, $R(75^\circ) \approx 0.38$. For small σ_{qs}, $\rho_{qs}(75^\circ) \approx R(75^\circ)$; $\rho_{qs}(75^\circ)$ decreases if σ_{qs} increases. If divergence of the reflected beam is negligible, incidence angles for the next reflections (except for the last, 6th, reflection) will be smaller. For the appreciably divergent reflected beam, we will observe a complicated distribution of rays by incidence angles after several successive reflections. This distribution determines the average normal effective emissivity values for small values of r.

Monotonic growth of the effective emissivities with r increasing is attributed to the divergence of the reflected beam. If r is increased (for a fixed σ_{qs}), a fraction of rays that hit cavity diaphragm and continue to reflect inside the cavity grows. When σ_{qs} grows, the quasi-specular lobe becomes wider, the fraction of rays hitting cavity walls instead of escaping through

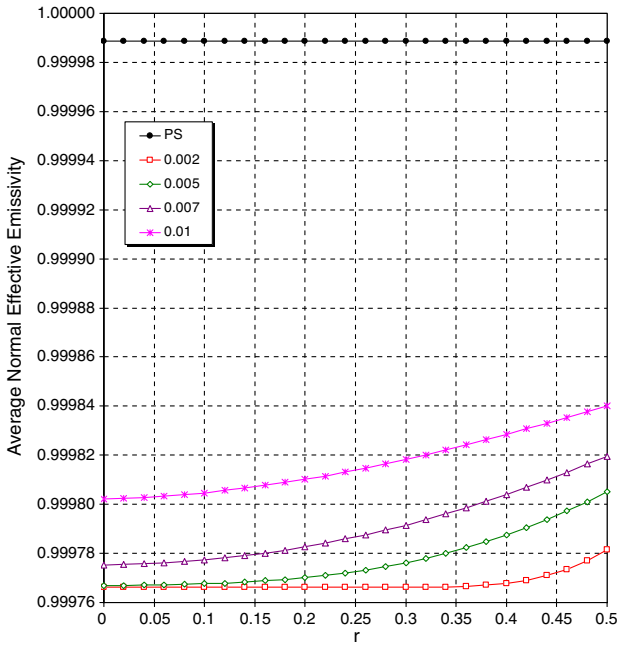

Fig. 8. (Color online) Average normal effective emissivities versus viewing beam radius for the cylindro-conical cavity with quasi-specular walls; $R_{qs} = 0.2$; $\sigma_{qs} = 0.002$, 0.005, 0.007, and 0.01 (see the legend; PS denotes perfectly specular case with the reflectance of 0.2)

the aperture also increases, and the average normal effective emissivity begins to rise at the smaller values of r.

C. Cavity with Glossy Walls

When studying glossy reflection, the conical effective emissivities of a cylindrical cavity were computed (Fig. 7b). Cylinder is the classical geometric shape for cavities with Lambertian walls. However, there is no reason to manufacture cylindrical cavity from a material with significant specular reflection because the effective emissivity along the axis of such a cavity won't be high enough. It was supposed that cavity walls are glossy and the apex of ray cone coincides with the cavity aperture center.

Figure 9 shows the conical effective emissivities computed against the viewing cone angle A for $R_g = 0.1$ and $\sigma_g = 0.2$, 0.3, 0.4, and 0.5. For comparison, the dependence obtained for the same cavity with purely diffuse reflectance $\rho = 0.1$ also is shown. The curve for diffuse case is higher than those for glossy cases with any reasonable σ_g so the effective emissivities of cylindrical cavities computed in diffuse approximation may be overestimated in some cases.

D. Comparison of 3C and USD Models

To determine whether the USD model at some values of ρ and D reproduces effective emissivities computed using the 3C model, we computed conical effective emissivities for cylindro-conical cavity shown in Fig. 7c. We synthesized 3C model with the following parameters: $k_d = 0.2$, $k_{qs} = 0.3$, $k_g = 0.5$,

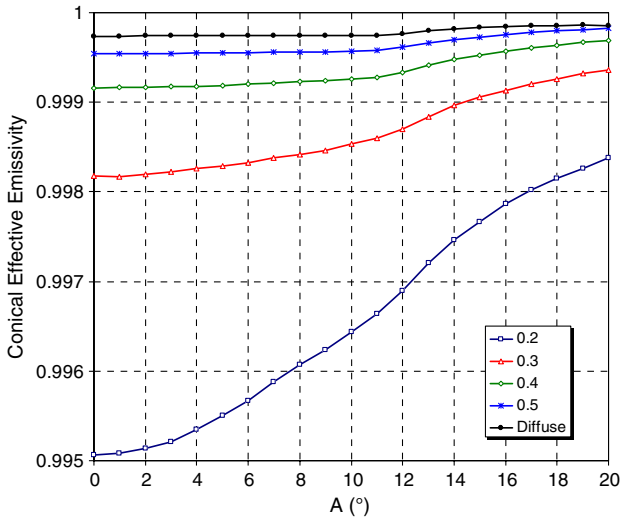

Fig. 9. (Color online) Dependences of the conical effective emissivities on the viewing cone angle computed for cylindrical cavity with glossy walls; $R_g = 0.1$, $\sigma_g = 0.2$, 0.3, 0.4, and 0.5 (see legend). Curve for diffuse cavity at $\rho = 0.1$ is shown for comparison.

$R_d = R_{qs} = R_g = 0.2$, $\sigma_{qs} = 0.003$, $\sigma_g = 0.03$. BRDFs of this model are presented in Fig. 10; computed DHRs for the entire model and its components are shown in Fig. 11. This model was applied to the cavity walls.

We also computed conical effective emissivities for the USD models with $\rho = 0.1$ and $\rho = 0.37$ (this corresponds to the DHR of 3C model at the incidence angle of 75°) and three diffusity values: $D = 0$, 0.5, and 1. We present the results in Fig. 12, but won't discuss the behavior of each curve in this graph. One thing is certain: the USD model does not reproduce results obtained using the 3C model. This conclusion is not all-embracing. We also encountered many cases where the USD model leads to results that are very close to those obtained with the 3C model. However, one principal disadvantage of the USD model remains in force for all cases: it is

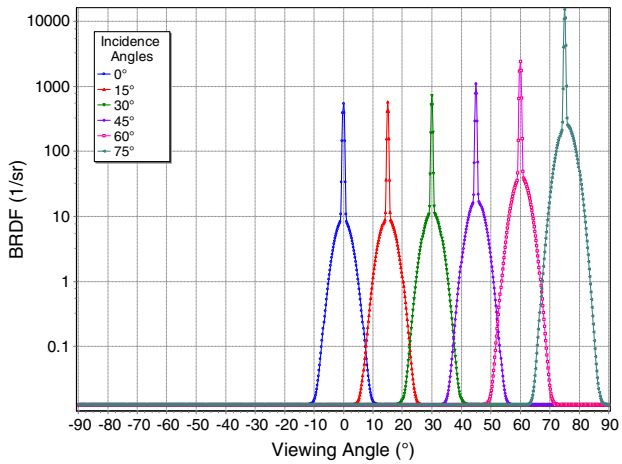

Fig. 10. (Color online) In-plane Cartesian plots of BRDFs for the 3C model used in numerical experiments. The negative values of viewing angles correspond to the backscattering.

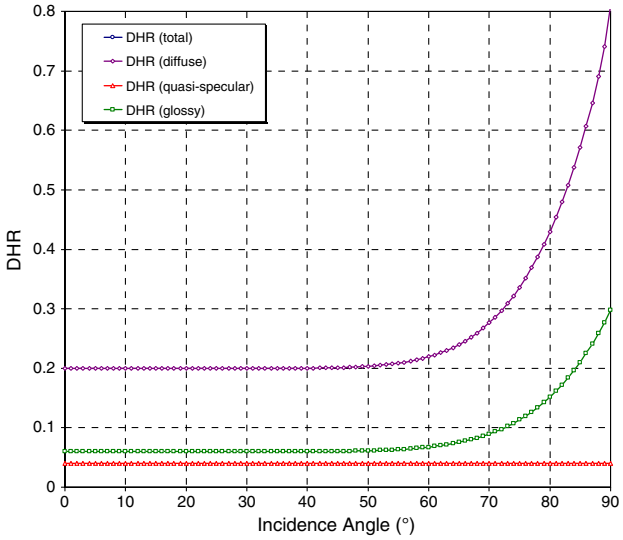

Fig. 11. (Color online) Dependences of DHR on the incidence angle for the 3C BRDF model and its components (see legend) used in numerical experiments.

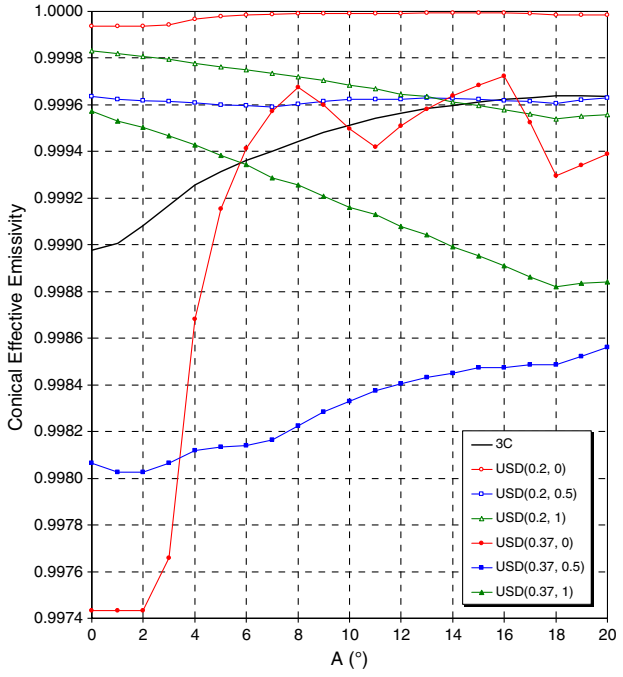

Fig. 12. (Color online) Dependences of the conical effective emissivities on the viewing cone angle A computed for cylindro-conical cavity for the 3C BRDF model with $k_d = 0.2$, $k_{qs} = 0.3$, $k_g = 0.5$, $R_d = R_{qs} = R_g = 0.2\,\sigma_{qs} = 0.003$, $\sigma_g = 0.03$ and for the USD model (in the legend: the first number bracketed denotes ρ, the second denotes D).

impossible to unambiguously subdivide reflectance onto diffuse and specular component. Therefore, it is impossible to choose the diffusity value that unambiguously results in correct effective emissivities.

7. Conclusion

The 3C BRDF model was proposed and studied in this work. A general outline for a suggested approach to fitting 3C model to measured BRDFs was given. The 3C BRDF model was incorporated into Monte Carlo ray-tracing algorithm for calculation of the effective emissivities of blackbody cavities. We investigated influence of the 3C model parameters on effective emissivities of blackbody cavities with simple geometric shapes and compared the results with those obtained using the conventional USD model of reflection. We found that there are cases when the USD model of reflection cannot reproduce results obtained using 3C BRDF model.

The USD model remains highly valuable in assessment of effective emissivities of blackbody cavities especially at the design stage, due to the minimal number of model's parameters and the simplicity of the interpretation of the results obtained. However, in some cases, the USD model might be too crude for precise characterization of blackbody calibration sources. This, in turn, may affect the measurement precision of such quantities as spectral radiance and radiance temperature.

In the future works, we plan to extend our analysis to isothermal cavities and introduce normalized modified version of the RPV model instead of the Lambertian component.

References

1. J. Hollandt, J. Seidel, R. Klein, G. Ulm, A. Migdall, and M. Ware, "Primary sources for use in radiometry," *Optical Radiometry*, A. C. Parr, R. U. Datla, and J. L. Gardner, eds. (Academic, 2005), pp. 213–290.
2. J. Hartmann, J. Hollandt, B. Khlevnoy, S. Morozova, S. Ogarev, and F. Sakuma, "Blackbody and other calibration sources," *Radiometric Temperature Measurements. I. Fundamentals*, Z. M. Zhang, B. K. Tsai, and G. Machin, eds. (Academic, 2010), pp. 241–295.
3. F. J. Kelly, "On Kirchhoff's law and its generalized application to absorption and emission by cavities," J. Res. Natl. Bur. Stand. B **69**, 165–171 (1965).
4. R. E. Bedford, "Calculation of effective emissivities of cavity sources of thermal radiation," *Theory and Practice if Radiation Thermometry*, D. P. DeWitt and G. D. Nutter, eds. (Wiley, 1988), pp. 653–772.
5. A. V. Prokhorov, L. M. Hanssen, and S. N. Mekhontsev, "Calculation of the radiation characteristics of blackbody radiation sources," in *Radiometric Temperature Measurements: I. Fundamentals*, Z. M. Zhang, B. K. Tsai, and G. Machin, eds. (Academic, 2010), Vol. 42, pp. 181–240.
6. A. Ono, "Calculation of the directional emissivities of the cavities by the Monte Carlo method," J. Opt. Soc. Am. **70**, 547–554 (1980).
7. M. J. Ballico, "Modeling of the effective emissivity of a graphite tube black body," Metrologia **32**, 259–265 (1995).
8. K. A. Snail, D. P. Brown, J. P. Costantino, W. C. Shemano, C. W. Schmidt, W. F. Lynn, C. L. Seaman, and T. R. Knowles, "Optical characterization of black appliqués," Proc. SPIE **2864**, 465–474 (1996).
9. M. J. Persky, "Review of black surfaces for space-borne infrared systems," Rev. Sci. Instrum. **70**, 2193–2217 (1999).
10. S. R. Meier, "Characterization of highly absorbing black appliqués in the infrared," Appl. Opt. **40**, 2788–2795 (2001).
11. S. R. Meier, "Reflectance and scattering properties of highly absorbing black appliqués over a broadband spectral region," Appl. Opt. **40**, 6260–6264 (2001).
12. J. Hartmann, "High-temperature measurement techniques for the application in photometry, radiometry and thermometry," Phys. Rep. **469**, 205–269 (2009).
13. F. E. Nicodemus, J. C. Richmond, J. J. Hsia, I. W. Ginsberg, and T. Limperis, "Geometrical considerations and nomenclature

for reflectance," NBS Monograph 160 (U.S. Department of Commerce, National Bureau of Standards, 1977).
14. A. S. Glassner, *Principles of Digital Image Synthesis* (Morgan Kaufmann, 1995), Vol. II.
15. P. Shirley, *Fundamentals of Computer Graphics* (A K Peters, 2002).
16. P. Dutré, P. Bekaert, and K. Bala, *Advanced Global Illumination* (A K Peters, 2003).
17. M. Pharr and C. Humphreys, *Physically Based Rendering: from Theory to Implementation* (Morgan Kaufmann, 2010).
18. M. Kurt and D. Edwards, "A survey of BRDF models for computer graphics," Comput. Graphics **43**, 4 (2009).
19. K. Schwenk, "A survey of shading models for real-time rendering," http://www.karsten-schwenk.de/downloads/a_survey_of_shading_models.pdf (2011).
20. O. Engelsen, B. Pinty, M. M. Verstraete, and J. V. Martonchik, "Parametric bidirectional reflectance factor models: evaluation, improvements and applications" (Space Applications Institute, Joint Research Centre, European Commission, ECSC-EC-EAEC, 1996).
21. S. Liang, *Quantitative Remote Sensing of Land Surfaces* (Wiley, 2004).
22. D. L. B. Jupp, "A compendium of kernel and other (semi-)empirical BRDF models" (CSIRO Office of Space Science Applications—Earth Observation Centre, 2000), http://www.eoc.csiro.au/tasks/brdf/k_summ.pdf.
23. A. F. Sarofim and H. C. Hottel, "Radiation exchange among non-Lambert surfaces," J. Heat Transfer **88C**, 37–44 (1964).
24. J. Zeng and L. Hanssen, "Development of an infrared optical scattering instrument from 1 μm to 5 μm," Proc. SPIE **7453**, 7453Q1 (2009).
25. L. M. Hanssen and A. V. Prokhorov, "Stochastic modeling of non-Lambertian surfaces for Monte Carlo computations in optical radiometry," Proc. SPIE **7427**, 742707 (2009).
26. L. M. Hanssen, S. N. Mekhontsev, J. Zeng, and A. V. Prokhorov, "Evaluation of blackbody cavity emissivity in the infrared using total integrated scatter measurements," Int. J. Thermophys. **29**, 352–369 (2008).
27. J. S. Liu, *Monte Carlo Strategies in Scientific Computing* (Springer, 2001).
28. D. Geisler-Moroder and A. Dür, "A new ward BRDF model with bounded albedo," Comput. Graph. Forum **29**, 1391–1398 (2010).
29. K. E. Torrance and E. M. Sparrow, "Theory for off-specular reflection from roughened surfaces," J. Opt. Soc. Am. **57**, 1105–1114 (1967).
30. C. Schlick, "An inexpensive BRDF model for physically based rendering," Comput. Graph. Forum **13**, 233–246 (1994).
31. P. van Dooren and L. de Ridder, "An adaptive algorithm for numerical integration over an n-dimensional cube," J. Comp. Appl. Math. **2**, 207–217 (1976).
32. M. Clerc, *Particle Swarm Optimization* (ISTE, 2006).
33. M. Clerc and J. Kennedy, "The particle swarm—explosion, stability, and convergence in a multidimensional complex space," IEEE Trans. Evol. Comput. **6**, 58–73 (2002).
34. A. S. Glassner, "An overview of ray tracing," in *An Introduction to Ray Tracing* A. S. Glassner, ed. (Academic, 1993), pp. 1–32.
35. E. M. Sparrow and R. D. Cess, *Radiation Heat Transfer* (Hemisphere, 1978).